Draft version February 5, 2008
Preprint typeset using LaTeX style emulateapj v. 04/21/05

MOLECULAR GAS, KINEMATICS, AND OB STAR FORMATION IN THE SPIRAL ARMS OF THE SOUTHERN MILKY WAY

A. Luna[1,2], L. Bronfman[2], L. Carrasco[1], and J. May[2]

Draft version February 5, 2008

ABSTRACT

The rotation curve for the IV galactic quadrant, within the solar circle, is derived from the Columbia University - U. de Chile CO(J=1→0) survey of molecular gas. A new sampling, four times denser in longitude than in our previous analysis, is used to compute kinematical parameters that require derivatives w/r to galactocentric radius; the angular velocity $\Omega(R)$, the epicyclic frequency $\kappa(R)$, and the parameters $A(R)$ and $B(R)$ describing, respectively, gas shear and vorticity. The face-on surface density of molecular gas is computed from the CO data in galactocentric radial bins for the subcentral vicinity, the same spectral region used to derive the rotation curve, where the two-fold ambiguity in kinematical distances is minimum. The rate of massive star formation per unit area is derived, for the same radial bins, from the luminosity of IRAS point-like sources with FIR colors of UC HII regions detected in the CS(J=2→1) line. Massive star formation occurs preferentially in three regions of high molecular gas density, coincident with lines of sight tangent to spiral arms. The molecular gas motion in these arms resembles that of a solid body, characterized by constant angular velocity and by low shear and vorticity. The formation of massive stars in the arms follows the Schmidt law, $\Sigma_{MSFR} \propto [\Sigma_{gas}]^n$, with an index of $n = 1.2 \pm 0.2$. Our results suggest that the large scale kinematics, through shear, regulate global star formation in the Galactic disk.

Subject headings: Galaxy: kinematics and dynamics — structure, ISM: molecules, stars: formation

1. INTRODUCTION

The rotation curve, describing the circular speed of rotating material as a function of galactocentric radius, is a fundamental tool for the study of the kinematics of our Galaxy. It is best derived, because of interstellar extinction, from observations of atomic and molecular gas in radio and mm wavelengths. The derivation involves determining the *terminal velocity*, or maximum absolute radial velocity relative to the Sun, toward lines of sight that sample the Galaxy within the solar circle (quadrants I and IV). Such terminal velocities correspond, assuming pure circular motion, to the tangent points to circumferences around the galactic center, named *subcentral points*. These points subtend a circumference that connects the solar position with the galactic center. A detailed analysis of the rotation curve can reveal important physical characteristics of the rotating material, such as the amount of shear and vorticity at each galactocentric radius. These physical quantities regulate the gravitational stability of a differentially rotating gaseous disk and, consequently, the large scale distribution and properties of star formation in the galactic disk.

The first derivation of the rotation curve for the IV galactic quadrant that made use of the CO(J=1→0) line - the best tracer of molecular hydrogen in the interstellar medium - was presented by Alvarez, May, & Bronfman (1990). The spectral data used to determine the terminal velocities were taken from the Columbia - U. de Chile surveys (Grabelsky et al. 1987; Bronfman et al. 1989), which have a sampling interval of $0°.125$ (roughly the beam size). However, the terminal velocities in Alvarez et al. (1990) were measured only every $0°.5$ in galactic longitude, due to difficulties involved in the visual examination of a very large number of spectra. A new derivation of the rotation curve, that uses a computer search code to examine all the available spectra (≈15000), is presented here. The disk kinematic characteristics in the IV galactic quadrant are analyzed in detail, from this new rotation curve. These characteristics, as a function of galactocentric radius, are compared with the molecular gas density and with the local rate of massive star formation.

A proper derivation of the spiral pattern of our Galaxy requires knowledge of the distances to the adopted tracers. These distances are also required to compute the masses and luminosities of such tracers. For the gas, kinematical distances can be obtained from radial velocity data of radio line observations, adopting a rotation curve, under the assumption of pure circular motions. For clouds within the solar circle, however, there is a two-fold ambiguity in the kinematic distance, that is difficult to circumvent and has to be resolved in a case-by-case basis. But in the vicinity of the subcentral points such ambiguity is minimal, since at the subcentral points themselves the kinematic distances are univocally defined.

It is worth noting that large scale streaming motions in spiral arms, with amplitude of ∼10 km/s, which produce deviations from pure rotation, have been observed in a number of regions of the Galaxy (Burton et al. 1988). Streaming motions of such amplitude may introduce uncertainties of up to 5% in the estimation of galactocentric radii when the streaming is along the line of sight. In such unfavorable case, the corresponding uncertainties in the estimated distances, for the section of the Galaxy analyzed here, may go from of 0.6 kpc to 1.7 kpc. In any case, for objects beyond ~ 3 kpc from the Sun, because of

[1] Instituto Nacional de Astrofísica Optica y Electrónica, Tonantzintla, Puebla, México; aluna@inaoep.mx, carrasco@inaoep.mx
[2] Departmento de Astronomía, Universidad de Chile, Casilla 36-D, Santiago, Chile; leo@das.uchile.cl, jmay@das.uchile.cl

optical extinction, kinematical distances are usually the only ones available.

Massive stars are formed within aggregates of molecular gas and dust of 10^5-10^6 solar masses, about 50-100 pc in size, which are commonly known as giant molecular clouds, or GMCs for short. The association between OB stars and the interstellar medium has been established through optical, infrared, and CO observations of GMCs close enough to be largely unaffected by extinction (Orion, Carina, etc). The physical conditions in GMCs control their rates of OB star formation, and are one of the main agents that regulate the evolution of the galactic disk (Evans 1999).

There is a close relationship between the galactic spiral structure and the formation of GMCs and, hence, with the formation rate of OB stars (Dame et al. 1986; Solomon et al. 1986). Therefore, the GMCs and the regions of OB star formation provide a very good tool to trace the spiral arm pattern of a galaxy. An early description of the Milky Way spiral arm pattern was given by Georgelin & Georgelin (1976), who observed the H109α line emitted in HII regions associated with young massive stars. A four arm spiral pattern for the southern Milky Way was later proposed by Caswell & Haynes (1987), using a larger observational database of hydrogen recombination lines (H109α & H110α). The four arm spiral pattern is in general agreement with that obtained from HI and CO large scale observations of the Galaxy (Robinson et al. 1983; Grabelsky et al. 1987; Bronfman et al. 1988; Alvarez et al. 1990; Vallée 2002).

Star formation is likely to occur in regions where the gas in the Galactic disk is unstable to the growth of gravitational perturbations. In a classical paper, Schmidt (1959) introduced the parametrization of the volume density of star formation and the volume density of gas, relating them through a power law; such parametrization, known as "Schmidt Law", has been studied observationally (Kennicutt 1989; Wong & Blitz 2002) and explained on theoretical grounds (Toomre 1964; Tan 2000). A study of the gas stability in the galactic disk must include (a) comparison of the gas density with a critical value above which the gaseous aggregates undergo gravitational collapse (Toomre 1964; Kennicutt 1989) and (b) examination of the gas shear rate, that governs the process of destruction of molecular clouds (e.g. Kenney, Carlstrom, & Young 1993; Wong & Blitz 2002), presumably through the injection of turbulent motions (Mac Low & Klessen 2004).

The link between massive star formation and kinematical conditions in disks has been studied mostly for external spiral galaxies (Aalto et al. 1999; Wong & Blitz 2002; Bosssier et al. 2003), where the spatial resolution that can be achieved by the observations is not as good as for the Milky Way. The main goal of the present paper is, therefore, to accurately describe the spiral arm structure in the *subcentral vicinity* of our Galaxy, focusing on the molecular gas kinematics, density, and on the rate of massive star formation, with the hope of contributing to the understanding of the formation and evolution of disk galaxies in general. The analysis is carried out for the IV galactic quadrant, where the spiral structure is more evident (Bronfman et al. 1988) than in the I quadrant. Preliminary work has been presented by Carrasco & Serrano (1983) and, more recently by Luna et al. (2001).

Section (§2) describes the observational datasets used, the most complete available in their kind. These data are used in section (§3) to derive the rotation curve and analyze the relation between molecular gas kinematics, molecular gas surface density, and massive star formation rate. The validity of Schmidt Law for the Milky Way is analyzed in section (§4), and a summary of the results is given in section §5.

2. OBSERVATIONS

The data used to derive the rotation curve and the molecular gas surface density are part of the Columbia-U. Chile ^{12}CO(J=1→0) surveys. These surveys provide us with the most extensive and homogeneous observational dataset of CO emission in the galactic disk (Grabelsky et al. 1987; Bronfman et al. 1989; Dame et al. 2001). The beam-size of the antenna in the CO line is $8'.8$, and an angular sampling of $0^\circ.125$ was adopted. The surveys cover the entire IV galactic quadrant in longitude, and $\pm 2^\circ$ in latitude about the galactic equator. The velocity resolution is $1.3\,\mathrm{km\,s^{-1}}$, and the typical rms noise antenna temperature of the observations is 0.1 K. Main beam temperatures, T_{MB}, are used throughout the analysis, obtained by dividing the antenna temperature T_A^* by the main beam efficiency, $T_{MB} = T_A^*/\eta_{MB}$, with $\eta_{MB} = 0.82$ (Bronfman et al. 1989). Hereinafter we refer to the ^{12}CO(J=1→0) line as CO. For a detailed description of the observations see Grabelsky et al. (1987) and Bronfman et al. (1989).

The rate of massive star formation is estimated from the integrated FIR luminosity (Boulanger & Perault 1988) of IRAS point-like sources, with FIR colors of UC HII regions (Wood & Churchwell 1989), detected in a CS(J=2→1) survey of 1427 sources in the whole Galaxy by Bronfman, Nyman, & May (1996). The CS(J=2→1) emission line requires high molecular gas densities, of 10^4 - $10^5\,\mathrm{cm^{-3}}$, to become excited. Therefore, it constitutes a good tracer of massive star forming regions. The survey used here is the most complete currently available, listing 843 massive star forming regions in the galactic disk; the observed velocity profiles provide a good estimator of kinematical distances to the sources.

The observations of the CS(J=2→1) line toward the IV galactic quadrant were obtained with the SEST (Swedish-ESO Sub-millimeter Telescope) at La Silla Observatory, in Chile, with a beam-size of 50". Typical rms noise in the spectra is 0.1 K, at a velocity resolution of $0.52\,\mathrm{kms^{-1}}$. The radial velocity coverage is $260\,\mathrm{kms^{-1}}$, large enough to detect all the sources in the radial velocity range allowed within the solar circle. Hereinafter we refer to the CS(J=2→1) transition as CS , and to the IRAS point-like sources detected in CS as IRAS/CS sources. A number of 66 sources from the Bronfman et al. (1996) survey are used in the present analysis. This number was complemented with 13 sources, undetected in the original CS survey, yet detected in a new CS survey with three times better sensitivity, completed with the SEST telescope, to be published elsewhere.

The present analysis adopts the IAU recommended values for the galactocentric distance of the Sun and for the solar circular velocity, i.e. $R_0 = 8.5\,\mathrm{kpc}$ and $V_0 = 220\,\mathrm{kms^{-1}}$ respectively (Kerr & Lynden-Bell 1986). The analysis excludes galactic longitudes from 350° to

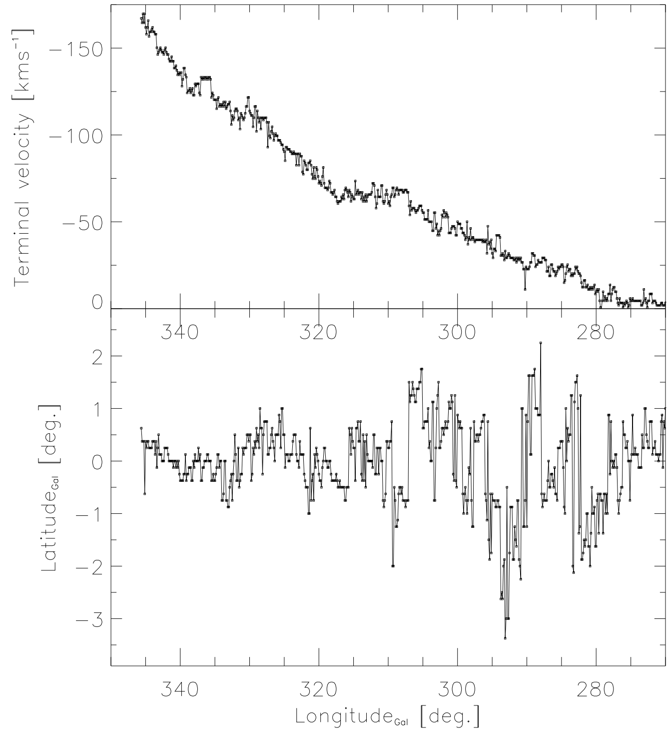

FIG. 1.— Terminal velocities in the IV galactic quadrant. *Top*: Measurements obtained every (0.°125) in Galactic longitude. *Bottom*: galactic latitude where each measurement was obtained.

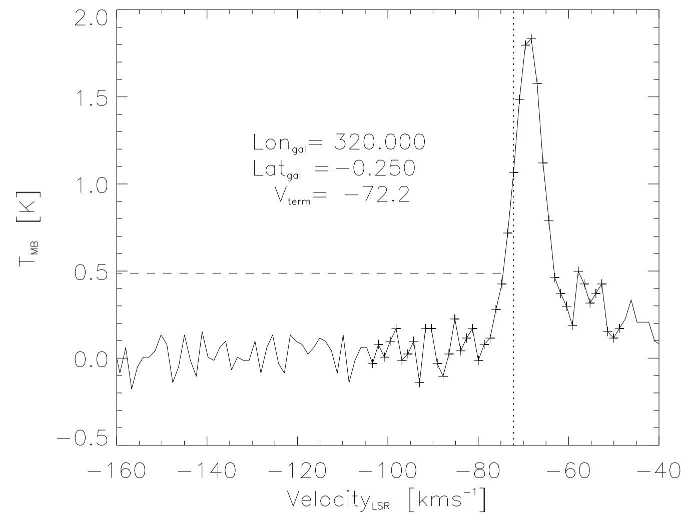

FIG. 2.— The detail of a typical spectrum (l = 320.000, $b = -0.250$) showing our selection criterion in velocity and temperature. The portion of the spectral velocity zone analyzed is marked with crosses at the measured temperature. For this feature, the maximum temperature is $T = 1.83K$ at $v = 67.8km\,s^{-1}$. The terminal velocity value $V_{term} = -72.2km\,s^{-1}$ is selected at the half-maximum temperature in the blue-shifted side of the line, and is indicated by the vertical dotted line. A 4σ noise level is indicated by the horizontal dashed line.

360°, because the method used to derive the kinematical distance is highly uncertain for that region. Furthermore, the kinematics of the central region of the Milky Way are more complex than those of the galactic disk (Sawada et al. 2001).

3. ANALYSIS

3.1. *Derivation of the rotation curve*

The rotation curve is derived from *terminal velocities* of CO spectra at each sampled galactic longitude l. Since the emission in the IV quadrant is blue-shifted, the most negative velocity is recorded, as well as the galactic latitude b where it occurs (Fig. 1). To define the terminal velocity, following work by Sinha (1978) for HI and by Alvarez et al. (1990) for CO, the half intensity point of the blue-shifted side of the emission peak with the most negative velocity is selected (Fig. 2). To be considered, an emission peak is required to be larger than 4 times the noise temperature T_{rms}. The emission lines thus selected have an average peak temperature of $1.8 \pm 0.7\,$K, and an average HWHM of $3 \pm 0.8\,$kms^{-1}.

The rotation curve is obtained from the set of terminal velocities by assigning to every longitude a subcentral point of galactocentric distance $R = R_0 \mid \sin(l) \mid$ and heliocentric distance $D = R_0 \cos(l)$. The rotational velocity is then derived for each subcentral point, and assigned to the galactocentric radius $R = R_0 \mid \sin(l) \mid$, under the assumption of (a) pure circular motions and (b) differential rotation with angular velocity not growing with galactocentric radius (Sofue & Rubin 2001). The rotation curve obtained, shown in Figure 3 (*top*), is similar to that derived by Alvarez et al. (1990), but more detailed; the agreement for the longitude range covered in both studies is better than $\pm 2\,$km$\,$s^{-1} (rms). A slight difference is apparent in the radial range R/R_0 = [0.56,0.62], where their analysis yields a systematic shift in velocity of $2\,$km$\,$s^{-1}.

The distance $Z \equiv R\tan(b)$ of the subcentral point to the galactic plane (Fig. 3 *bottom*) is also determined, for each longitude, providing a simple tool to examine the Z distribution of the CO emission as a function of galactocentric radius. The results obtained compare well with those by Alvarez et al. (1990), which adopted the same method, and with those obtained from an axisymmetric analysis of the CO emission in the IV quadrant (Bronfman et al. 1988).

3.2. *Disk kinematics*

The rotation curve contains vast amount of information about the kinematics of the galactic disk (Binney & Tremaine 1987). Among the principal parameters characterizing the kinematics, derived here, are $A(R)$ and $B(R)$, which describe the radial trends of shear and vorticity, respectively; these parameters, when evaluated at $R = R_0$, correspond to the well known Oort's constants.

As observed from a non-inertial coordinate frame, e.g. that centered on the Sun (Local Standard of Rest, LSR), the balance between Coriolis, centrifugal, and gravitational forces induce non-circular orbits about the galactic center. These motions can be described as small periodic oscillations superimposed onto circular orbits. In a coordinate frame with its origin in the galactic center and corotating with the solar orbit, these periodic oscillations trace small ellipses called *epicycles*, with an associated *epicyclic frequency*, κ, which roughly accounts for deviations from circular motion. The value of $\kappa(R)$ depends, at each galactocentric radius, on the angular velocity $\Omega(R)$:

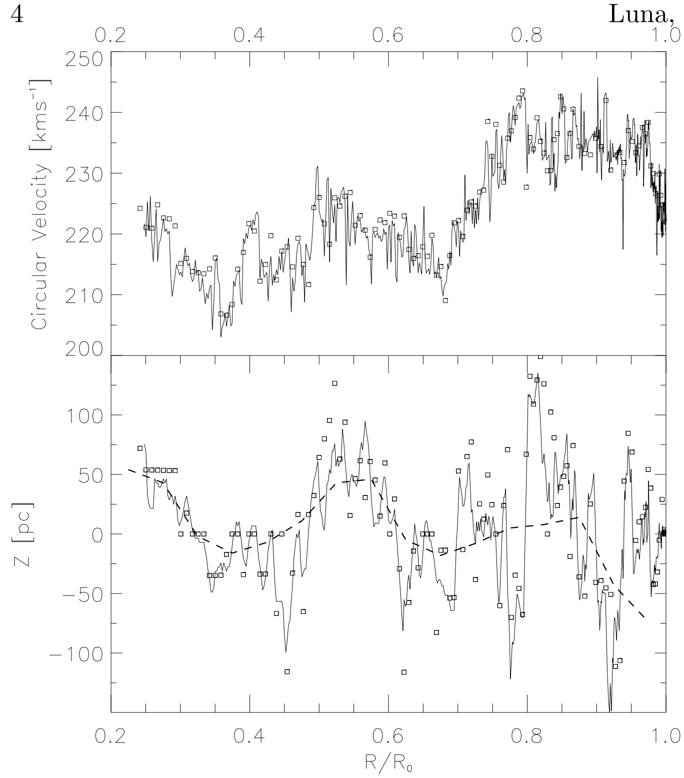

FIG. 3.— Rotation curve for the galactic quadrant IV. *Top:* In our present analysis, shown by the thin line, the longitude resolution is four times better than in Alvarez et al. (1990), shown by small squares. The rms difference for positions analyzed in both studies is 2 $\mathrm{km\,s^{-1}}$. *Bottom:* Our results for the position Z of the subcentral point w/r to the galactic equator (thin line), are fairly consistent with those obtained by Alvarez et al. (1990), shown by small squares, and with the emission centroid Z_0 obtained by Bronfman et al. (1988) through an axisymmetric analysis of the full quadrant IV CO dataset. (dashed line).

$$[\kappa(R)]^2 = 4[\Omega(R)]^2 \left[1 + \frac{1}{2}\frac{R}{[\Omega(R)]}\left(\frac{d[\Omega(R)]}{dR}\right)_R\right], \quad (1)$$

or, using the Oort's A and B parameters in their general definition (Binney & Tremaine 1987),

$$A(R) = -\frac{1}{2}R\frac{[d\Omega(R)]}{dR} \quad , \quad B(R) = -\Omega(R) + A(R), \quad (2)$$

it is possible to write the epicyclic frequency as:

$$\kappa(R) = \sqrt{-4[B(R)][A(R) - B(R)]}. \quad (3)$$

A smoothed version of the rotation curve (Fig. 4 *top*) is used in the calculation, in order to provide continuity for the derivative of $\Omega(R)$ with respect to R . The size of the smoothing box is 0.5 kpc, smaller than the typical width of spiral arms. There are three galactocentric radial regions, marked in Fig. 4 *top*, where $V(R)$ increases monotonically, so that the radial derivative is positive and roughly constant, i.e. the signature of solid body rotation. The kinematical parameters $A(R)$, $B(R)$, $\kappa(R)$, and $\Omega(R)$, as functions of galactocentric radius, are shown in Figure 4 (*bottom*).

The angular velocity, $\Omega(R)$, the epicyclic frequency, $\kappa(R)$, and the parameter $A(R)$, describing the shear, decrease on the average with galactocentric radius. On the contrary, the parameter $B(R)$, describing the vorticity,

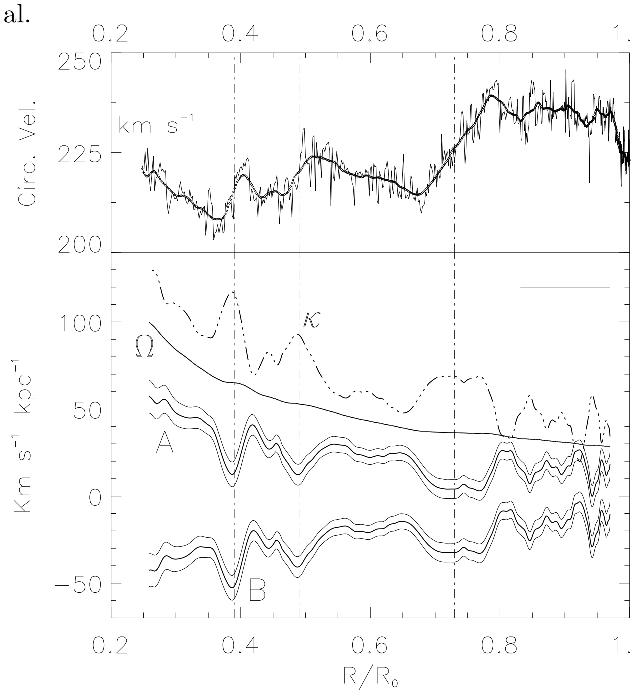

FIG. 4.— Rotation curve and derived kinematical parameters. The vertical lines depict the center of the regions presumably with solid-body rotation *Top*: A box size of 0.5 kpc has been used to obtain a boxcar smoothed version (thick line) of the measured rotation curve (thin line). *Bottom*: The epicycle frequency $\kappa(R)$, the angular velocity $\Omega(R)$, and the Oort parameters $A(R)$ and $B(R)$, derived from the smoothed version of the rotation curve. The 1σ errors in $A(R)$ and $B(R)$ are shown with thin lines. The segment from 0.83 to 0.97 R/R_0 (shown at $120 km\,s^{-1}$ in the plot) is the radial region used to fit the Oort constants A and B.

grows with galactocentric radius. The shear and vorticity present three relative minima, coincident with local maxima of the epicyclic frequency $\kappa(R)$, at radii 0.39, 0.47 and 0.73 R/R_0. The parameter $A(R)$, directly proportional to the radial derivative of the angular velocity, tends to zero at these radii, so the angular velocity is almost constant, a characteristic of solid body rotation. The relative maxima in $\kappa(R)$ at these three radii can be interpretated also as evidence for solid body rotation; at a given galactocentric radius, κ would be $\sqrt{2}$ times higher for solid body rotation than for a flat rotation curve $V(R) = V_0 =$ constant.

The results of our analysis are consistent with other work in that the parameters $A(R)$ and $B(R)$ at $R = R_0$, are very close to the values of the Oort's constants A_0 and B_0 recommended by the IAU (Kerr & Lynden-Bell 1986). The values derived here are obtained from linear fits to $A(R)$ and $B(R)$, within the range 0.83 to $0.97 R/R_0$, extrapolated to $R/R_0 = 1$. Our results yield $A_0 = 14.9 \pm 4\ \mathrm{km\,s^{-1}\,kpc^{-1}}$, and $B_0 = -12.3 \pm 4\ \mathrm{km\,s^{-1}\,kpc^{-1}}$, in good agreement with those recommended by the IAU, $A_0 = 14.5 \pm 2\ \mathrm{km\,s^{-1}\,kpc^{-1}}$ and $B_0 = -12.0 \pm 3\ \mathrm{km\,s^{-1}\,kpc^{-1}}$. In a similar manner a value of $\kappa_0 = 35 \pm 7 \mathrm{km\,s^{-1}\,kpc^{-1}}$ is obtained for the epicyclic frequency at $R = R_0$, in agreement with the value of $\kappa_0 = 36 \pm 10\ \mathrm{km\,s^{-1}\,kpc^{-1}}$ given by Binney & Tremaine (1987). The angular velocity obtained for $R = R_0$, $\Omega_0 = 27.2 \pm 1\ \mathrm{km\,s^{-1}\,kpc^{-1}}$, is comparable with the value of $\Omega_p = 26 \pm 4\ \mathrm{km\,s^{-1}\,kpc^{-1}}$, derived for the spiral pattern angular velocity (Fernández, Figueras, & Torra 2001). Our results therefore suggest

that the Sun location is close to the corotation radius (see also discussion in Amaral & Lepine 1997).

3.3. *The subcentral vicinity*

To study the possible relationships between the kinematical characteristics of the Galaxy, the molecular gas density distribution and the massive star formation rates (MSFR), it is necessary to use consistent data sets. The densities and MSFRs should be estimated, preferentially, for the very same regions for which the kinematics have been inferred. The rotation curve is obtained using information from the subcentral points of the disk, so the densities and MSFRs we wish to examine are evaluated in regions adjacent to the subcentral points. Such procedure advantageously minimizes the two-fold ambiguity in kinematical distance occurring within the solar circle since, at the subcentral points, kinematical distances are univocally defined (Binney & Tremaine 1987).

Limiting the analysis to a reduced area of the longitude-velocity space avoids also the azimuthal averaging of physical conditions which pertain both to spiral arms and to inter-arm regions, a difficulty that appears in axisymmetric analysis of the entire longitude-velocity space. Azimuthal averaging, over disk annuli, of the gas surface density and star formation rates, allows derivation of the star formation activity threshold in disk galaxies (Martin & Kennicutt 2001; Bosssier et al. 2003); the detailed information on the spiral structure of the disk, however, is washed out in the azimuthal average.

The "*subcentral vicinity*", used to inspect the gas physical conditions and MSFR, is defined here, at each galactic longitude, as the velocity span between the terminal velocity and the terminal velocity plus $\Delta V = 15\,\mathrm{km\,s^{-1}}$ (Fig. 5). The value of $15\,\mathrm{km\,s^{-1}}$ is large enough to include all the emission from each CO profile component used to select a terminal velocity. Were the emission to be interpreted as originated by a set of clouds at different velocities, the range ΔR implied by $\Delta V = 15\,\mathrm{km\,s^{-1}}$ would be 0.5 kpc at $l = 307°$ and 0.2 kpc at $l = 342°$, roughly the longitude limits of the analyzed region. These values of ΔR are small compared to the large scale trends with respect to galactocentric radius and therefore do not affect our conclusions.

The properties of the ISM, molecular gas face-on surface density and MSFR per unit area, are averaged within the subcentral vicinity, to evaluate their dependance on galactocentric radius. It is assumed that the gas shares the kinematics of the corresponding subcentral point at each longitude. The molecular gas face-on surface density is computed from the same CO database used to derive the rotation curve, while the MSFR is computed from the FIR luminosity of the IRAS/CS sources.

3.4. *Molecular gas surface density*

The derivation of molecular clouds mass from our CO survey data is based on the widely made assumption that the velocity-integrated CO intensity is directly proportional to the total H_2 column density in molecular clouds, and is therefore proportional (with a correction to account for helium) to the total molecular gas mass column density. (Binney & Tremaine 1987). To evaluate the molecular gas surface density, Σ_{gas}, the CO emission is binned in galactocentric annuli of thickness

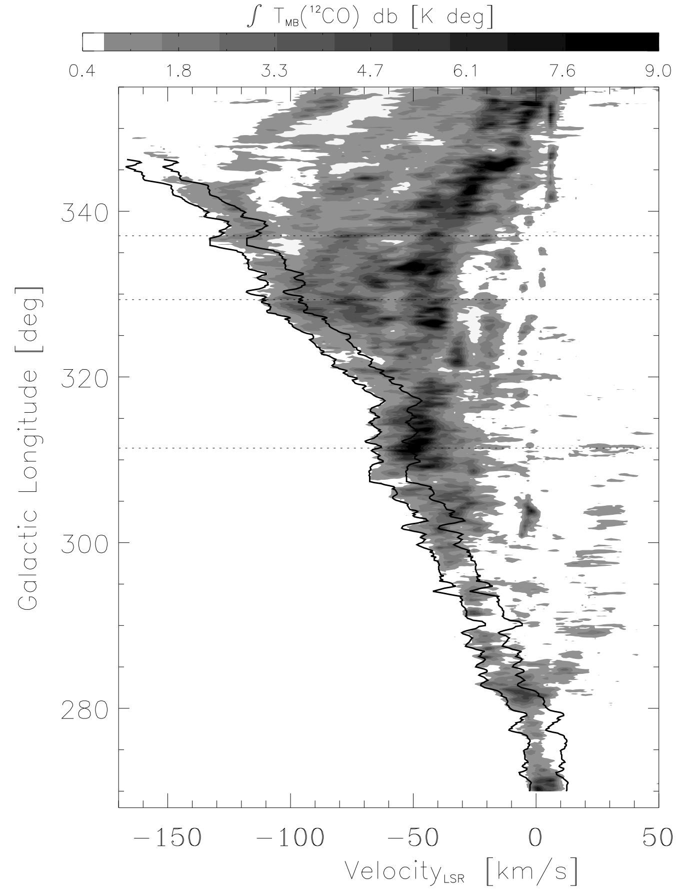

FIG. 5.— The subcentral vicinity borders, separated by $\Delta V = 15 km\,s^{-1}$ are shown with the thick lines atop the longitude-velocity diagram of CO emission (gray scale), integrated in latitude over $-2° \leq b \leq 2°$. Horizontal dotted lines mark the regions with solid body rotation, as in Figure 4.

$0.05\,R/R_0$ and, for each radial bin, integrated over all velocities within the subcentral vicinity and over $[-2°, 2°]$ in latitude. The resultant quantity is divided by the sampled face-on area. The proportionality factor X adopted, where $\mathrm{N(H_2)} = XW(^{12}\mathrm{CO})$, is equal to 1.56×10^{20} cm^{-2} $(\mathrm{K\,km\,s^{-1}})^{-1}$, (Hunter et al. 1997). A correction of 1.36 is used to account for helium (see Murphy & May 1991). The results obtained for the gas surface density in the subcentral vicinity, within the solar circle, are shown in Figure 6 (*top*).

3.5. *Rate of massive star formation*

Massive stars form in the dense cores of giant molecular clouds. The UV radiation from the young stars heats the surrounding dust, which re-radiates the energy principally in the far infrared. Most of these cores are detected as IRAS point-like sources, with FIR colors typical of ultra-compact HII regions (Wood & Churchwell 1989). The density is high enough for the excitation of the CS line, above 10^4 - $10^5\,\mathrm{cm^{-3}}$ (Bronfman et al. 1996). Following Kennicutt (1998a), the rate of massive star formation as a function of galactocentric radius is computed by adding the FIR luminosity of the IRAS/CS sources that fall within each radial bin.

$$MSFR_{FIR} = 6.5 \times 10^{-10} \left(\frac{L_{FIR}}{L_\odot}\right) [M_\odot yr^{-1}]. \quad (4)$$

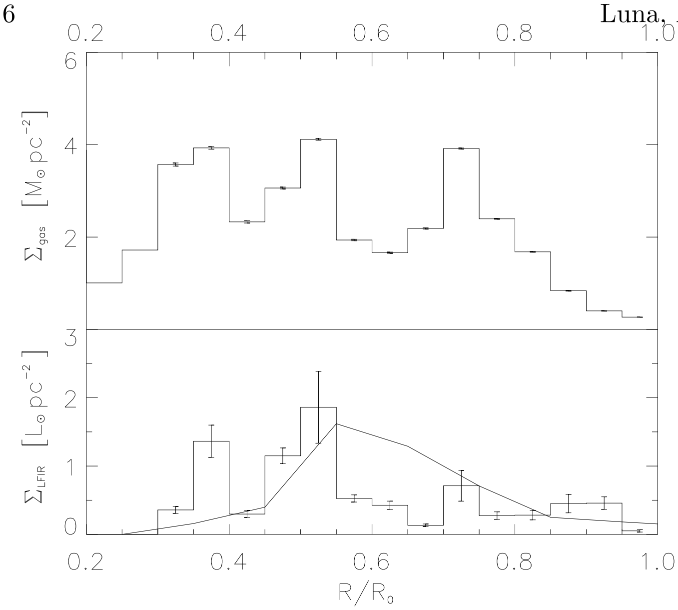

FIG. 6.— Molecular gas surface density and integrated FIR luminosity from massive star forming regions. *Top*: The face-on surface density for the subcentral vicinity. *Bottom*: Integrated FIR luminosity per unit face-on area for the subcentral vicinity compared with an axisymmetric analysis of the southern galactic disk (Bronfman et al. 2000). The analysis of the subcentral vicinity shows structure related with the spiral pattern.

The FIR luminosity is evaluated as $L_{FIR} = 4\pi D^2 F_{FIR}$ (Boulanger & Perault 1988), where D is the subcentral distance,

$$F_{FIR} = \sum_{i=1}^{4} \nu F_\nu(i), \tag{5}$$

and $F_\nu(i)$ are the FIR fluxes of the IRAS/CS point-sources in the four IRAS bands, as published in the Point Source Catalog. The galactic FIR face-on surface luminosity of IRAS/CS sources as a function of galactocentric radius, for the subcentral vicinity, is presented in Figure 6 (*bottom*), compared with the axisymmetric analysis of the complete southern galactic disk by Bronfman et al. (2000).

The FIR surface luminosity estimated here for massive star forming regions constitutes only a lower limit, since the emitting regions powered by embedded massive stars can be more extended than the IRAS resolution. But deconvolution of the extended FIR continuum emission can be much more difficult because of superposition of sources along the line of sight. For point-like sources there is no such confusion since all the CS profiles measured have only one velocity component (Bronfman et al. 1996) and, therefore, the derivation of kinematical distances is straightforward.

The derived MSFR per unit area (Figure 7*c*) has relative maxima at the same galactocentric radial regions than the molecular gas surface density (Fig. 7*b*). These radial regions are characterized by solid-body like rotation, as shown in the smoothed version of the rotation curve displayed in (Fig. 7*a*).

3.6. *Gravitational disk stability*

The Toomre criterion for disk stability (Toomre 1964; Binney & Tremaine 1987), used here, is described through the Q stability parameter for gas, defined by

$$Q(R) = \frac{\alpha c \kappa(R)}{\pi G \Sigma_{gas}(R)}, \tag{6}$$

where c is the velocity dispersion, G is the gravitational constant, Σ_{gas} is the gas surface density and α is a dimensionless parameter that accounts for deviations of real disks from the idealized Toomre thin disk, single fluid model (Tan 2000). When $Q < 1$ a gaseous disk is gravitationally unstable. The particular case $Q = 1$ defines a critical surface density value, governed by the Coriolis force represented by $\kappa(R)$;

$$\Sigma_{crit}(R) = \frac{\alpha c \kappa(R)}{\pi G}. \tag{7}$$

The Toomre parameter Q can be expressed, hence, as $Q = \Sigma_{crit}/\Sigma_{gas}$. The constant α is usually estimated defining $Q = 1$ where massive star formation ceases along disks of galaxies (Kennicutt 1998b; Hunter et al. 1998; Pisano et al. 2000). Here a value of $\alpha = 0.08$ is found by defining $Q = 1$ in the galactocentric radial range $R/R_0 =$ 0.4 to 0.45, where the MSFR per unit area is close to zero. Following (Kennicutt 1998b), a value of $6\,\mathrm{km\,s^{-1}}$ is adopted for the velocity dispersion. The dependance of Q on galactocentric radius is shown in Figure 7*d*.

To analyze the case of cloud destruction governed by the shear rate instead of the Coriolis force, Toomre's criterion has been modified by Elmegreen (1993). The shear rate is described by the Oort parameter $A(R)$; a new parameter, Q_A, that evaluates the survival of a cloud, is in this case

$$Q_A(R) = \frac{\alpha_A 2.5 c A(R)}{\pi G \Sigma_{gas}(R)}, \tag{8}$$

Clouds are sheared to destruction, in differentially rotating disks, for gas surface densities larger than the critical surface density Σ^A_{crit}

$$\Sigma^A_{crit}(R) = \frac{2.5 \alpha_A c A(R)}{\pi G}, \tag{9}$$

so that $Q_A = \Sigma^A_{crit}/\Sigma_{gas}$. This modified stability criterion takes into account the important role of shear in the destruction of GMCs, and can be used to describe how shear controls the rate of star formation in galactic disks in the regions where the Coriolis force does not. The parameter α_A is found, as α, to be $\alpha_A = 0.2$. The dependance on galactocentric radius of Q_A is shown in Figure 7*e*.

A complementary analysis of the stability of the gas clouds to tidal shear is proposed by Kenney et al. (1993), who defines a critical tidal surface density Σ_{tide}.

$$\Sigma_{tide}(R) = \frac{\sigma_z(R)[3A(A-B)]^{1/2}}{\pi G}, \tag{10}$$

where σ_z is the velocity dispersion in the z-direction of the disk. If the gas density is less than Σ_{tide}, tidal shear will rip apart the clouds. The relative importance of tidal shear and gravitational stability can be expressed by the ratio of Σ_{tide} to the critical surface density for gravitational instabilities as defined by Toomre for an ideal disk,

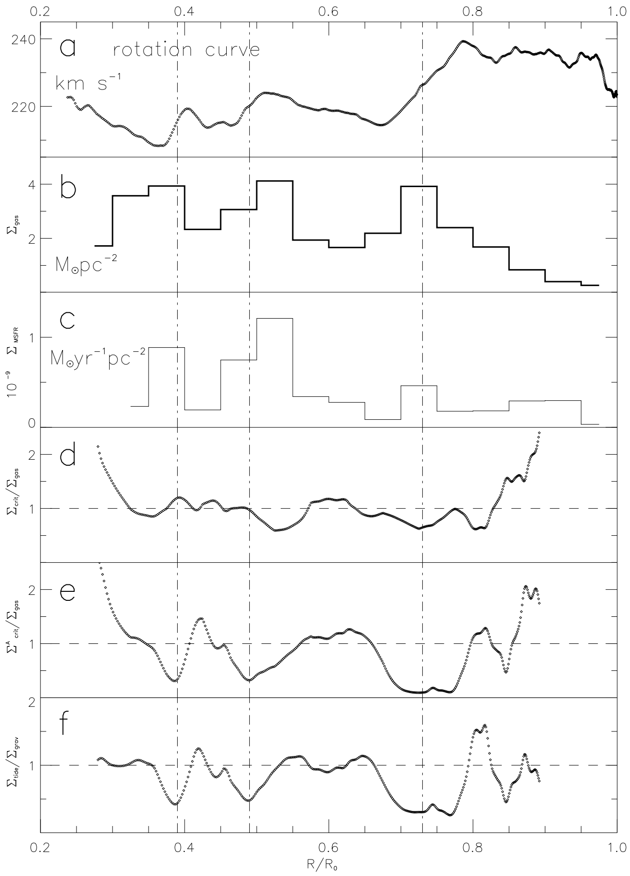

FIG. 7.— Summary of the results from our analysis of the subcentral vicinity. The regions with solid-body like kinematics are shown by vertical dash-dotted lines. Correlations are discussed in the text. (*a*) Smoothed rotation curve. (*b*) Molecular gas face-on surface density (*c*) Massive star formation rate per unit area Σ_{MSFR}. (*d*) Gravitational instability parameter $\Sigma_{crit}/\Sigma_{gas}$. (*e*) shear instability parameter $\Sigma^A_{crit}/\Sigma_{gas}$. (*f*) Parameter $\Sigma_{tide}/\Sigma_{grav}$ comparing the relative influences of gravity and tide in the disk stability.

$$\Sigma_{grav} = \frac{c\kappa}{\pi G}. \tag{11}$$

Assuming that $c \approx \sigma_z$, the ratio depends almost entirely on the shape of the rotation curve,

$$\frac{\Sigma_{tide}}{\Sigma_{grav}} = 0.87\left(\frac{-A}{B}\right)^{1/2}, \tag{12}$$

and tells whether tidal or gravitational forces determine the disk stability. The dependance of $\Sigma_{tide}/\Sigma_{grav}$ in galactocentric radius is shown in Figure 7*f*.

3.7. *Disk stability, gas density, and massive star formation*

Some of our most relevant results are displayed in Figure 7, which we now describe in more detail. The values plotted and their errors are also listed in Table 1. Panel *a*, depicts the smoothed rotation curve used to derive the Oort parameters $A(R)$ and $B(R)$. Uncertainties in the rotation curve, of $\pm 2\,\mathrm{km\,s^{-1}}$, are dominated by the deviation of the measured subcentral velocities from the smoothed curve. Panel *b* presents the molecular gas face-on surface density evaluated in galactocentric radial bins of extent $0.05R/R_0$, with the first bin centered at $R/R_0 = 0.275$. Panel *c* shows the MSFR, in units of solar masses per year per square pc (Σ_{MSFR}), averaged in the same galactocentric radial bins as for *b*. Uncertainties are estimated from Poisson statistics. Panel *d* displays the gravitational stability parameter Q defined by Toomre; panel *e* the Q_A parameter defined by Elmegreen (1993) for the case when shear dominates over Coriolis force; and panel *f*, finally, the ratio of the tidal to the gravitation surface instabilities (eq. [11]). The ratio *f* is estimated from the parameters $A(R)$ and $B(R)$ derived from observed rotation curve.

The gas surface density and the MSFR are higher than average, as apparent from Figure 7, in regions where the rotation is typical of a solid body, roughly indicated by the vertical lines at radii 0.39, 0.47 and $0.73R/R_0$ (see also Fig. 4). These three regions are very close to the accepted values for the tangent points of spiral arms identified in the literature (e.g. Vallée 2002 and references therein); the 3 kpc arm approximately at $0.36R/R_0$, the Norma spiral arm at $0.51R/R_0$ and the Crux spiral arm at $0.77R/R_0$. Figure 7*d* tells us that although gravitational instabilities are present in the Galactic disk, the disk is self-regulated in the sense that Q is of order 1 everywhere (Tan 2000). However, as shown in Figure 7*e*, where the Coriolis force is replaced by shear as the principal agent of cloud destruction, the three regions coincident with spiral arm tangents are characterized by relative minima. This result is reinforced by the three relative minima in Figure 7*f*, where the tidal shear is clearly lower than that needed to disrupt the clouds and, therefore, allows them to survive enough so as to collapse gravitationally and ultimately form massive stars.

To estimate the influence of the derived quantities and parameters in the process of massive star formation, we examine the correlation between Σ_{MSFR} (Panel *c*) and Σ_{gas}, $\Sigma_{crit}/\Sigma_{gas}$, $\Sigma^A_{crit}/\Sigma_{gas}$, $\Sigma_{tide}/\Sigma_{grav}$, Ω and κ. A Spearman rank-order correlation coefficient test (Press et al. 1992) is adopted; the ranking and significance of each correlation are listed in Table 2. Massive star formation is clearly correlated with the gas surface density, with a confidence level larger than 90%, and less clearly correlated with the angular velocity and the epicyclic frequency, with a confidence level larger than 75% and lower than 85%. For the variables $\Sigma^A_{crit}/\Sigma_{gas}$ and $\Sigma_{tide}/\Sigma_{grav}$, which take into account shear, there is no correlation with respect to the NULL hypothesis that the dependent variables are drawn from a random distribution. These results are discussed in the following section, searching for a possible scenario to explain the observed correlations.

4. DISCUSSION

4.1. *Spiral arms in the Southern Galaxy*

There are regions in the rotation curve (Fig. 7*a*) that present solid-body like kinematics; these regions are coincident with the loci of known spiral arm tangents. The molecular gas surface density is at least a factor of 2 larger for the arm regions than for the inter-arm regions (Fig. 7*b*). In those regions where the rotation is typical of a solid body, the rate of massive star formation per unit area, Σ_{MSFR}, presents relative maxima (Fig. 7*c*). The relative maxima in the molecular gas surface den-

sity and MSFR are coincident with relative minima in the kinematical parameters $\Sigma^A_{crit}/\Sigma_{gas}$ and $\Sigma_{tide}/\Sigma_{grav}$. Such results, as shown in Figure 6*b*, cannot be obtained alone from an axisymmetric analysis of the Galactic disk.

In those radial regions where the kinematics resembles that of a solid body, i.e., spiral arm tangents, marked with vertical lines in Figure 7, $V/R = \Omega \approx$constant and $-A/B \ll 1$. Stability analysis suggests that molecular gas in regions characterized by solid body rotation is stable ($\Sigma_{gas} \approx \Sigma_{crit}$) or self-regulated (Tan 2000); GMCs are not destroyed by tidal disruption ($\Sigma_{tide} \ll \Sigma_{gas}$), and there is an enhancement in Σ_{MSFR}. In regions that deviate from solid body rotation, the star formation decreases, implying that shearing motions may disrupt/destroy clouds and, therefore, play an important role in regulating large scale star formation in the disk.

The destruction of clouds by shearing motions, therefore, is an important parameter controlling the large scale star formation in the disk, particularly in the inter-arm regions where shear dominates gravitational stability. High tidal disruption appears to be the agent for GMC destruction in the inter-arm regions, inhibiting the formation of massive stars, while low tidal disruption facilitates the accumulation of gas in the arms, increasing the gas surface density locally and promoting the higher observed MSFR. Regions of solid body rotation should present less collisions due to the low shearing motions and, therefore, the MSFR could presumably be limited by a process different from shear.

The relation between solid body motion and enhanced star formation has been also found for external galaxies. A nearby example of a galaxy in which shear instability may regulate star formation is M33 (Corbelli 2003; Heyer et al. 2004). Using a shear stability criterion, they find that the predicted outer threshold radius for star formation is consistent with the observed drop in the Hα surface brightness. Another example is the central region of NGC 3504. The molecular gas kinematics are derived by Kenney et al. (1993), and compared with the rate of star formation obtained from the Hα recombination line. The central region of NGC 3504 is characterized by solid body kinematics and high rate of star formation; they propose that the behavior of star formation is strongly influenced by the strength of tidal shear, which can help control the star formation rate via cloud destruction. For irregular galaxies, Hunter et al. (1998) notice that in slowly raising rotation curves, characteristic of this type of galaxies, the stability parameter derived by Elmegreen (1993) (eq. 8), provides a good criterion to describe the boundary between cloud survival and disruption. The conclusions of these authors are similar to our results for the Southern Milky Way arms, which show solid body kinematics, i.e. that the SF is strongly influenced by tidal shear, and in particular that tidal shear controls the rate of star formation through cloud destruction.

Theoretical work in agreement with the present results has been presented by Roberts & Stewart (1987). They use a galactic disk model where the ISM is simulated by a system of particles, representing clouds, which orbit in a one arm spiral-perturbed gravitational field, and include dissipative cloud-cloud collision. Their conclusion is that the distribution of GMCs and star formation is enhanced across the full finite width of the spiral arm and is not restricted to either the preshock or postshock regions.

The agreement between their theoretical results and our observations implies that the best tracer for molecular gas spiral structure is the kinematical parameter that compares gravitational stability and cloud shear destruction ($\Sigma_{tide}/\Sigma_{grav}$, Fig. 7*f*), and is also the simplest one, because it involves only kinematical parameters that can be derived directly from the rotation curve. Spiral arm regions can be identified, therefore, as those where shear disruption of clouds has less influence than gravitational instabilities, so that molecular clouds can pile up, increasing their mass and evolving, until they collapse to form stars that will thereby increase the mean kinetic temperature. Such increment in temperature in the spiral arm regions has been preliminarily measured by Luna et al. (2004).

4.2. *Massive star formation and the Schmidt Law*

There is a good correlation, as shown in section 3.7, between the MSFR per unit area (Fig. 7*c*) and the molecular gas face-on surface density (Fig. 7*b*) in the Milky Way. Such kind of correlation, formally known as Schmidt law, has been explored mostly for external galaxies. In this section we evaluate, for the sub-central vicinity of the Milky Way disk, four different enunciations of the Schmidt Law, whose simplest form (Kennicutt 1989) is, in our case,

$$\Sigma_{MSFR} \propto (\Sigma_{gas})^n, \tag{13}$$

Previous efforts at deriving the Schmidt Law for the Milky Way include those of Guibert et al. (1978), who find values of n between 1.3 and 2.0, based on the distribution of OB associations, H II regions, H I, and early CO surveys; and (Bosssier et al. 2003), who using known gaseous and stellar radial profiles, find that the Schmidt Law is satisfied for the Milky Way from R = 4 to 15 kpc. Recently (Krumholz & McKee 2005), in a general theory of turbulence-regulated star formation in galaxies, predict the star formation rate as a function of galactocentric radius for the Milky Way taking into account the fraction of molecular gas in the form of clouds, and enunciate Schmidt Law in the assumption that the clouds are virialized and supersonically turbulent.

A second form of the Schmidt law, which modulates the gas density by a kinematical parameter, in this case the angular velocity Ω (Kennicutt 1989), is given by

$$\Sigma_{MSFR} \propto \Sigma_{gas}\Omega. \tag{14}$$

A third derivation of the Schmidt Law (Tan 2000), can be expressed as

$$\Sigma_{MSFR} \propto \Sigma^n_{gas}\Omega(1 - 0.7\beta), \tag{15}$$

with

$$\beta \equiv \frac{d[\ln(v_{circ})]}{d[\ln(R)]}, \tag{16}$$

where v_{circ} is the circular velocity at a particular galactocentric radius. This version of Schmidt law has the advantage that the proportionality constant can be derived from theory, and includes evaluation of the mean

free path for cloud-cloud collision, the fraction of collisions that lead to star formation, and the fraction of gas transformed into stars in each collision.

A fourth derivation, of theoretical character, that assumes molecular clouds to be virialized and supersonically turbulent, has been given by Krumholz & McKee (2005), and is expressed here as

$$\Sigma_{MSFR} \propto f_{GMC} \Sigma_{gas}^{0.68} \Omega^{1.32}, \tag{17}$$

where f_{GMC} is the fraction of gas in the form of molecular clouds

The four enunciations of Schmidt Law are tested (Figure 8) using the values of molecular gas face-on surface density and of the MSFR per unit area obtained here for galactocentric radial bins in the Milky Way. Although most derivations of Schmidt Law include both atomic and molecular gas, our calculations are limited to the molecular gas component of the ISM. Wong & Blitz (2002) have found, for a set of seven galaxies, that the azimuthally averaged star formation rate per unit area correlates much better with Σ_{H_2} than with Σ_{HI}. One should note that they required a large, uncertain correction for extinction to derive the rate of star formation using Hα images; however, such correction does not affect their main conclusion, i. e., that considering the total gas density, rather than HI and H_2 separately, may obscure underlying physical processes that are essential to star formation. The situation may be presumably different in galaxies where the ISM is predominantly atomic; however, even for M33, with a predominantly atomic ISM, Heyer et al. (2004) has shown that the star formation rate per unit area still correlates better with Σ_{H_2} than with Σ_{HI}.

The Schmidt law is roughly satisfied in all four cases analyzed, with a power index close to 1. The dispersion of the data points is large if all radial bins are taken into account; however, the relation becomes much tighter if the radial bins that correspond to interarm regions, shown in Figure 8 as thin squares, are removed. For the simplest relation (Fig. 8*a*), $\Sigma_{gas} \propto (\Sigma_{MSFR})^n$, the index value $n = 1.2 \pm 0.2$ obtained is in good agreement with those derived for extragalactic disks (Wong & Blitz 2002). The relation plotted at Figure 8*b*, taking into account the kinematics through the angular velocity Ω, with an index value $n = 1.0 \pm 0.1$, is in very good agrement with Kennicutt (1998b). Because they derive an index from disk-averaged values for a set of galaxies, rather than the variation of star formation rate with surface density within a galaxy, presumably describing quite different processes, our results show an underlaying physical link between Σ_{gas} and Σ_{MSFR} that dominates both local and global scales in the process of star formation. The relation for the Schmidt law at Figure 8*c*, dependent on the kinematics, as proposed by Tan (2000), shows a relation with an index value $n = 1.4 \pm 0.2$, consistent with theory. An index of 1.2 ± 0.1 is obtained when fitting the relation derived by Krumholz & McKee (2005), using a value of $f_{GMC} = 0.25$ (Dame et al. 1987).

It is apparent that the simplest form (Fig. 8*a*) of Schmidt law, that normally describes the averaged properties of disks of galaxies (Kennicutt 1989), applies also fairly well to Σ_{MSFR} in a scale range which is much smaller, like the radial bins in the Milky Way. The galactic disk kinematics, through shear, additionally modulates the global star formation in the Galactic disk; destroys the clouds in the interarm regions and permits the piling up of gas in the spiral arms, allowing gravity or another agents like compression and turbulence (via supernovas), to collapse the clouds into stars (see recent reviews by Elmegreen (2002); Mac Low & Klessen (2004).

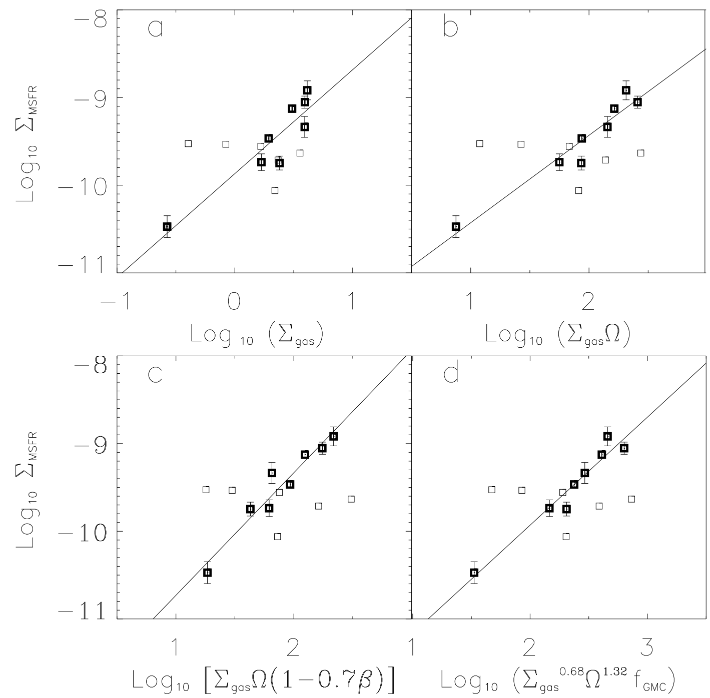

Fig. 8.— The Schmidt law, relating massive star formation rate and gas density in the subcentral vicinity of the Milky Way, obtained with four different methods. Thick squares represent spiral arm tangent regions and thin squares interarm regions. Linear fits to the radial bins corresponding to spiral arm regions yield tight correlations in all four cases (see text). (*a*) Simplest expression: $Log(\Sigma_{MSFR}[M_{\odot} yr^{-1} pc^{-2})$ vs $Log(\Sigma_{gas}[M_{\odot} pc^{-2})$. (*b*) Expression including the angular velocity explicitly, $Log(\Sigma_{gas}\Omega(R)[M_{\odot} yr^{-1} pc^{-2} kms^{-1} kpc^{-1}])$. (*c*) Expression derived by Tan (2000). (*d*) Expression derived by Krumholz & McKee (2005)

4.3. *Timescale for the growth of gravitational instabilities*

The gas depletion timescale due to star formation, τ_{SF}, can be crudely estimated from the derived MSFR per unit area, Σ_{MSFR}, and the molecular gas surface density, Σ_{gas},

$$\tau_{SF} = \frac{\Sigma_{gas}}{\Sigma_{MSFR}}. \tag{18}$$

The galactocentric trend of τ_{SF} is shown in Figure 9 (*top*). Its average value is 10^{10} yr, an upper limit since Σ_{MSFR} represents a lower limit. The timescale for growth of GMCs through gravitational instabilities can be expressed as $\tau \sim Q/\kappa$ (Larson 1988). Results here yield timescales of the order $\sim 10^7$yr, with relative minima at the location of the spiral arm tangents (Fig. 9 *middle*). Following Kenney et al. (1993), the efficiency of star formation (ϵ) can be estimated via $\tau_{SF}=\epsilon^{-1}\tau$ if the timescales for gravitational instabilities (τ) are similar to the timescale for cloud collapse. The values of

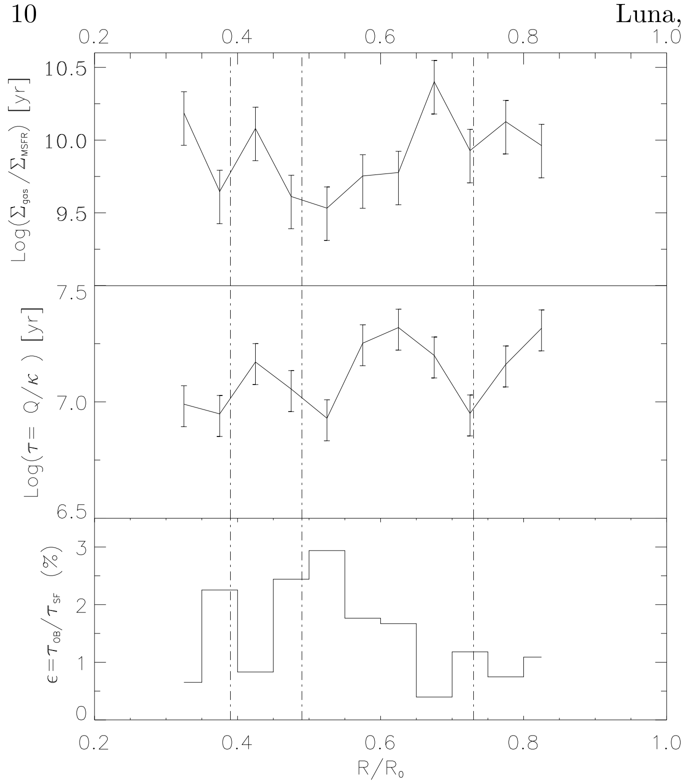

FIG. 9.— Comparison between galactocentric radial variations of the gas consumption time, the growth of gravitational instabilities, and the star formation efficiency. Vertical dash-dotted lines show regions with solid body - like kinematics (see text). (*Top*) Timescale for gas consumption due to star formation. (*Middle*) Timescale for gravitational instability growth. (*Bottom*) Star formation efficiency (percentage) using a constant 10^8 yr life time (τ_{OB}) for OB associations.

a few tenths of a percent obtained, however, are rather low as compared with values of a few percent typically reported in the literature.

The efficiency for massive star formation, according to Mac Low & Klessen (2004), can be further expressed as

$$\epsilon = \tau_{OB} \frac{\Sigma_{MSFR}}{\Sigma_{gas}} = \frac{\tau_{OB}}{\tau_{SF}}. \quad (19)$$

Adopting a typical lifetime for an OB star region of $\tau_{OB} = 10^8$yr and our results for Σ_{MSFR} and Σ_{gas} we obtain values for ϵ of a few percent in the spiral arms, and extremely low values for inter-arm regions, (Fig. 9 *bottom*). A comparison of the timescales of gas consumption and growth of gravitational instabilities, as a function of galactocentric radius, suggests that fast star formation is present in regions where rapid cloud growth takes place.

5. CONCLUSIONS

This work analyzes the correlation between molecular gas kinematical properties, molecular gas surface density, and rate of massive star formation in the IV galactic quadrant, using the most complete data bases available. The analysis is carried out for galactocentric radial bins 0.5 kpc wide, a compromise to avoid arm-interarm confusion while having good statistics. The data used are restricted to the subcentral vicinity, to avoid the two-fold distance ambiguity within the solar circle. The main conclusions are:

• The rotation curve obtained is similar to that presented by Alvarez et al. (1990). Since the sampling in longitude is 4 times denser, however, it can be used to calculate, as a function of galactocentric radius, kinematical parameters that require radial derivatives.

• The angular velocity, $\Omega(R)$, the epicyclic frequency, $\kappa(R)$, and the parameter $A(R)$ describing the gas shear, tend to decrease with galactocentric radius; the parameter $B(R)$, describing the gas vorticity, tends to grow. The values derived for Oort's constants A_0 and B_0, at R = R_0, are consistent with those recommended by the IAU.

• Shear and vorticity have relative minima, and the epicyclic frequency relative maxima, at radii 0.39, 0.47 and 0.73 R/R_0, coincident with the known positions of spiral arm tangent regions. Near these radii the kinematics are characteristic of solid body rotation: $A(R)$, proportional to the radial derivative of the angular velocity, tends to zero, so the angular velocity is roughly constant. The relative maxima in epicyclic frequency are consistent with such scenario since κ is $\sqrt{2}$ times higher for solid body rotation than for a flat rotation curve.

• Differential rotation and shear are weaker for the spiral arm regions than for the interarm regions. The relative importance of tidal shear w/r to gravitation in the stability of the gas for spiral arm regions, where the rotation curve resembles that of a solid body, is half than for spiral arms, where the rotation curve is nearly flat.

• Massive star formation occurs in regions of high molecular gas density, roughly coincident with the three lines of sight tangent to spiral arms. In these arms the formation of massive stars follows the Schmidt law, $\Sigma_{MSFR} \propto [\Sigma_{gas}]^n$, with an index of $n = 1.2 \pm 0.2$. While this law is characteristic of spiral galactic disks, here it applies to much smaller spatial scale. A modified version of Schmidt law, which modulates the gas density by the angular velocity, $\Sigma_{MSFR} \propto \Sigma_{gas}\,\Omega$, describes better the behavior of the gas at this scale, suggesting that the kinematics, through shear, regulate global star formation in the Galactic disk.

A.L. and L.C. acknowledge support by CONACYT México through the research grants 89964, 42609 and G28586. L.B., J.M., and A.L. acknowledge support from FONDECYT Grant 1010431 and from the Chilean *Center for Astrophysics* FONDAP No. 15010003. We thank Drs. E. Brinks, A. Garcia-Barreto, N. Vera and W. Wall for fruitful comments. A.L. thanks INAOE's Astronomy Department and is also grateful for the use of facilities and the support at the Departmento de Astronomía, Universidad de Chile. We are also grateful to the referee for several helpful comments.

REFERENCES

Aalto, S., Huttemeister, S., Scoville, N. Z., & Thaddeus, P. 1999, ApJ, 522, 165

Alvarez, H., May, J., & Bronfman, L. 1990, ApJ, 348, 495

Amaral, L. H., & Lépine, J. R. D. 1997, MNRAS, 286, 885

Binney, J., & Tremainen S. 1987, Galactic Dynamics (Princeton: Princeton Univ. Press)

Bossier, S., Prantzos, N., Boselli, A., and Gavazzi, G. 2003, MNRAS, 346, 1215

Boulanger, F., & Perault, M. 1988, ApJ, 330, 964
Bronfman, L., Cohen, R., Alvarez, H., May, J. & Thaddeus, P. 1988, ApJ, 324, 248
Bronfman, L., Alvarez, H., Cohen, R., & Thaddeus, P. 1989, ApJS, 71, 481.
Bronfman, L., Nyman, L.A., & May, J. 1996, A&A, 115, 81
Bronfman, L., Casassus, S., May, J., & Nyman, L.A. 2000, A&A, 358, 521
Burton, B. 1988, in Galactic and Extragalactic Radioastronomy, ed. G. L. Vershuur & K. I. Kellerman, (New York: Springer-Verlag) 295
Carrasco, L., & Serrano, A. 1983, IAU Symp. 100, Internal Kinematics and Dynamics of Galaxies, (Dordrech: Reidel), 135
Caswell, J., & Haynes, R. 1987, A&A, 171, 261
Corbelli, E. 2003, MNRAS, 342, 199
Dame, T., Elmegreen, B., Cohen, R., Thaddeus, R. 1986, ApJ, 305, 892
Dame, T., et al. 1987, ApJ, 322, 706
Dame, T., Hartmann, D., & Thaddeus, R. 2001, ApJ, 547, 792
Elmegreen, B. 1993, in Star Formation, Galaxies and the Interstellar Medium, ed. Franco, Ferrini, & Tenorio-Tagle, (Cambridge: Cambridge Univ. Press)
Elmegreen, B. 2002, ApJ, 577, 206
Evans, N.J. 1999, ARA&A37, 311
Fernández, D., Figueras, & F., Torra, J. 2001, A&A, 327, 833
Georgelin, Y.M., & Georgelin, Y.P. 1976, A&A, 49, 57
Grabelsky, D.A., Cohen, R.S., Bronfman, L., Thaddeus, P., & May, J. 1987, ApJ, 315, 122
Guibert, J., Lequeux, J., & Viallefond, F. 1978, A&A, 68, 1
Heyer, M., Corbelli, E., Schneider, S., & Young, J. 2004 ApJ, 602, 723
Hunter, S.D., Bertsch J.R., Catelli J.R. et al. 1997, ApJ481, 205
Hunter, D.A., Elmegreen B.G., Baker A.L. 1998, ApJ493, 595
Kenney, J., Carlstrom, J. and Young, J. 1993, ApJ, 418, 687
Kennicutt, R. 1989, ApJ, 344, 685
Kennicutt, R. 1998a, ARA&A, 36, 189
Kennicutt, R. 1998b, ApJ, 498, 541
Kerr, F.J., & Lynden-Bell D. 1986, MNRAS, 221, 1023
Krumholz, M.R., & McKee, C.F. 2005, ApJ630, 250
Larson, R. B. 1988, in Galactic and Extragalactic star Formation, ed. R. E. Pudritz & M. Fich (Dordrecht: Kluwer), 435
Luna, A., Carrasco, L., Wall, W., & Bronfman, L. 2001, ASP Conf. Ser. 275, Disks of Galaxies: Kinematics, Dynamics and Perturbations, ed. Athanassoula, Bosma, & Mújica (San Francisco: ASP), 131
Luna, A., Wall, W., Carrasco, L., Bronfman, L., & Hasegawa, T. 2004, II international workshop on science with the GTC: Science with GTC 1st-light instruments and the LMT, held in Cd. México, Mex., 16-18 febrero 2004, in press
Martin, C.L., & Kennicutt, R.C. 2001, ApJ, 555, 301
Mac Low, M.M., & Klessen, R.S. 2004, Reviews of modern physics, 76, 125
Murphy, D.C., & May, J. 1991, A&A, 555, 301
Pisano, D.J., Wilcots, E. M., & Elmegreen, B. 2000, ApJ, 120, 763
Press, W.H., Teukolsky, S.A., Veterling, W.T., Flannery, B.R. 1992, Numerical Recipes, The Art of Scientific Computing (Second Edition), Cambridge University Press
Roberts, W. W., & Stewart, G. 1987, ApJ, 314, 10
Robinson, B., McCuthcheon, W., Manchester, R., & Whiteoak, J. 1983, Surveys of the Southern Galaxy, ed. Burton & Israel, 1
Sawada, T., et al. 2001, ApJS, 136, 189
Schmidt, M. 1959 ApJ, 129, 243
Solomon, P.M., Sanders, D.B, & Rivolo, A.R. 1986, ApJ, 292, L19
Sellwood, J. A., & Balbus, S. A. 1978, ApJ, 511, 660
Sinha, R. P. 1978, A&A, 69, 227
Sofue, Y., & Rubin, V. 2001, ARA&A, 39, 137
Tan, J. 2000, ApJ, 536, 173
Toomre, A. 1964, ApJ, 139, 1217
Vallée, J. 2002, ApJ, 566, 261
Wong, T., & Blitz, L. 2002, ApJ, 569, 157
Wood, D.O.S., & Churchwell, E. 1989, ApJ, 340, 265

TABLE 1
VALUES OF OUR DERIVED AND MEASURED PARAMETERS IN THE ADOPTED BINS AT THE SUBCENTRAL VICINITY. OUR ANALYSIS BEYOND $0.875 R/R_0$ IS UNCERTAIN AND THEREFORE EXCLUDED.

Gal. radii [a]	circ. vel. [b]	Σ_{gas} [c]	$\Sigma_{MSFR}(10^{-9})$ [d]	$\Sigma_{crit}/\Sigma_{gas}$ [e]	$\Sigma^{A}_{crit}/\Sigma_{gas}$ [f]	$\Sigma_{tide}/\Sigma_{grav}$ [g]
R/R_0	kms^{-1} ±2	$M_\odot pc^{-2}$	$M_\odot yr^{-1} pc^{-2}$			
0.325	212.4	3.57 ±0.03	0.23 ±0.03	0.99 ±0.11	1.12 ±0.10	1.03 ±0.12
0.375	209.6	3.93 ±0.03	0.89 ±0.15	1.00 ±0.04	0.43 ±0.10	0.56 ±0.11
0.425	214.2	2.33 ±0.03	0.19 ±0.03	1.07 ±0.14	1.45 ±0.11	1.17 ±0.18
0.475	215.7	3.06 ±0.02	0.75 ±0.07	1.01 ±0.05	0.51 ±0.10	0.61 ±0.11
0.525	223.6	4.12 ±0.02	1.21 ±0.34	0.59 ±0.06	0.58 ±0.06	0.93 ±0.11
0.575	219.3	1.94 ±0.02	0.34 ±0.03	1.09 ±0.11	1.13 ±0.11	0.97 ±0.13
0.625	218.0	1.66 ±0.02	0.28 ±0.04	1.14 ±0.12	1.25 ±0.11	1.00 ±0.15
0.675	214.5	2.19 ±0.01	0.09 ±0.01	0.91 ±0.06	0.65 ±0.09	0.75 ±0.13
0.725	225.3	3.92 ±0.01	0.46 ±0.15	0.63 ±0.01	0.09 ±0.06	0.31 ±0.21
0.775	236.7	2.40 ±0.01	0.18 ±0.04	0.99 ±0.02	0.17 ±0.10	0.34 ±0.20
0.825	234.3	1.68 ±0.01	0.18 ±0.04	0.91 ±0.10	1.03 ±0.09	1.03 ±0.22
0.875	236.1	0.84 ±0.01	0.29 ±0.09	1.69 ±0.20	2.03 ±0.17	1.08 ±0.26
0.925	233.1	0.41 ±0.01	0.30 ±0.06	–	–	–
0.975	233.6	0.33 ±0.01	0.03 ±0.01	–	–	–

[a]Central bin position
[b]Circular velocity from the smoothed rotation curve at central bin position
[c]Averaged molecular gas surface density by bin
[d]Averaged rate of massive star formation, per unit area, by bin
[e,f,g]Stability parameters evaluated using the interpolated version of averaged surface quantities by bin, and the related kinematic parameter from the smoothed rotation curve at each position

TABLE 2
THE SPEARMAN TEST TO EXPLORE POSSIBLE CORRELATIONS BETWEEN Σ_{MSFR} AND Σ_{gas}, AS WELL AS BETWEEN Σ_{MSFR} AND KINEMATICAL AND INSTABILITY PARAMETERS PRESENTED IN TABLE 1.

correlation with Σ_{MSFR}	Σ_{gas}	$\Sigma_{crit}/\Sigma_{gas}$	$\Sigma^{A}_{crit}/\Sigma_{gas}$	$\Sigma_{tide}/\Sigma_{grav}$	Ω	κ
Rank	0.53	-0.02	-0.24	-0.26	0.41	0.36
confidence level	>90%	7%	55%	60%	82%	76%